Supplement of Atmos. Chem. Phys., 22, 13935–13947, 2022
https://doi.org/10.5194/acp-22-13935-2022-supplement

Atmospheric Chemistry and Physics
Open Access
EGU

Supplement of

Comprehensive characterization of particulate intermediate-volatility and semi-volatile organic compounds (I/SVOCs) from heavy-duty diesel vehicles using two-dimensional gas chromatography time-of-flight mass spectrometry

Xiao He et al.

Correspondence to: Xuan Zheng (x-zheng11@szu.edu.cn) and Ye Wu (ywu@mail.tsinghua.edu.cn)

Text S1. Authentic standards, internal standards, and instrumental analysis

The authentic standards include 25 *n*-alkanes (C_{13}-C_{37}), 6 *n*-alkenes (C_{10}, C_{12}, C_{14}, C_{16}, C_{18}, C_{20}), isophorone, 2 benzylic ketone esters, 2 cycloalkanes, 2-5 ring PAHs, 4 phenol benzylic alcohols, and 5 Nitros. The list of authentic standards is presented in Table S1

The internal standards used in this work include deuterated alkanes ($C_{12}D_{26}$, $C_{16}D_{34}$, $C_{20}D_{42}$, $C_{24}D_{50}$, $C_{28}D_{58}$, $C_{32}D_{66}$), deuterated PAHs (naphthalene-d_8, acenaphthene-d_{10}, phenanthrene-d_{10}, fluoranthene-d_{10}, chrylene-d_{12}, perylene-d_{12}, benzo(a)pyrene-d_{12}), cyclohexane-d_{12}, biphenyl-d_{10}, 1,3,5-trimethylbenzene-d_{12}, and *p*-xylene-d_{10}.

Text S2. Dynamic sampling of field blanks and the quality control/quality assurance

Field blank samples of background dilution air were collected simultaneously on each sampling day to correct for the blank matrix. Filtered ambient air was drawn into the constant volume sampler (CVS, MEXA-7200DTR) and deposited on quartz filter. To maintain consistency, blank sampling duration was 1800 s.

In previous studies, two common experimental settings are deployed to characterize the gas-particle (g-p) partitioning of vehicle emitted intermediate-volatility and semi-volatile organic compound (I/SVOCs). The first design places Tenax TA sampling tubes after quartz filters and particulate and gaseous I/SVOCs are collected separately (Zhao et al., 2015). The second design uses bare quartz filter (bare-Q) to collect total I/SVOC compounds and quartz filter behind Teflon filter (QBT) to collect gaseous I/SVOC compounds (May et al., 2013a, 2013b). The adsorption of gaseous I/SVOCs onto filters can cause negative biases in the measured gas phase concentrations and positive artifacts in the measured particle phase concentrations. In the former experimental design, the particulate I/SVOCs are positively biased due to the vapor loss to the quartz filters, whereas in the latter one, total I/SVOCs are negatively biased due to the insufficient collection of gaseous I/SVOCs by quartz filters. Comparing with quartz filters, which absorb vapours significantly (May et al., 2013b). Teflon has small surface area and is relatively inert. Considering the reasons stated above, a Teflon filter is deployed instead of a quartz filter before Tenax TA sampling tubes.

The uncertainties of the emission factors are assessed. First, the peak area or height of internal standards among different samples are highly reproducible, which reveals that the analytical method could be well duplicated. Second, the calibration curves for all the target compounds are well established. Third, the instrument blank tests were conducted throughout the whole experiment, and no blank contamination is observed. Forth, less than 1% signal intensity of the re-test sample was observed, confirming that the carry-over effect was not a concern. Last, it was reported that using surrogates would introduce un uncertainty of approximate 24% and 28.1%, which gives an overall idea of the uncertainty level of the quantification (Alam et al., 2018; Huo et al., 2021).

Text S3. The calibration and method detection limit for each authentic standard

The calibration curve for each authentic standard is built by spiking gradient volumes (0, 1, 2, 5, 7, 10 μL) of working solution plus 2 μL of internal standard solution and establishing a liner relationship between the peak area (PA) ratio (PA of each authentic standard/PA of the corresponding internal standard) and the spiked mass. The method detection limit (MDL) for each authentic standard is determined as half of the minimum mass on the calibration curve and is summarized in Table S1.

Text S4. Calculation of the saturation mass concentration

Saturation mass concentration (C_i^*) of individual *n*-alkane is calculated using the following equation:

$$C_i^* = \frac{M_i 10^6 \zeta_i P_{L,i}^0}{760RT}$$

where M_i is the molecular weight of species *i* (g mol^{-1}); ζ_i is the activity coefficient of species *i* in the condensed phase and is assumed to be 1; $P_{L,i}^0$ is the liquid vapor pressure (torr) for species *i*, which is obtained from the US EPA Suite data (https://www.epa.gov/tsca-screening-tools/download-epi-suitetm-estimation-program-interface-v411). R is the ideal gas constant (8.2 ×10^{-5} m^3 atm mol^{-1} K^{-1}); T is the air temperature (K).

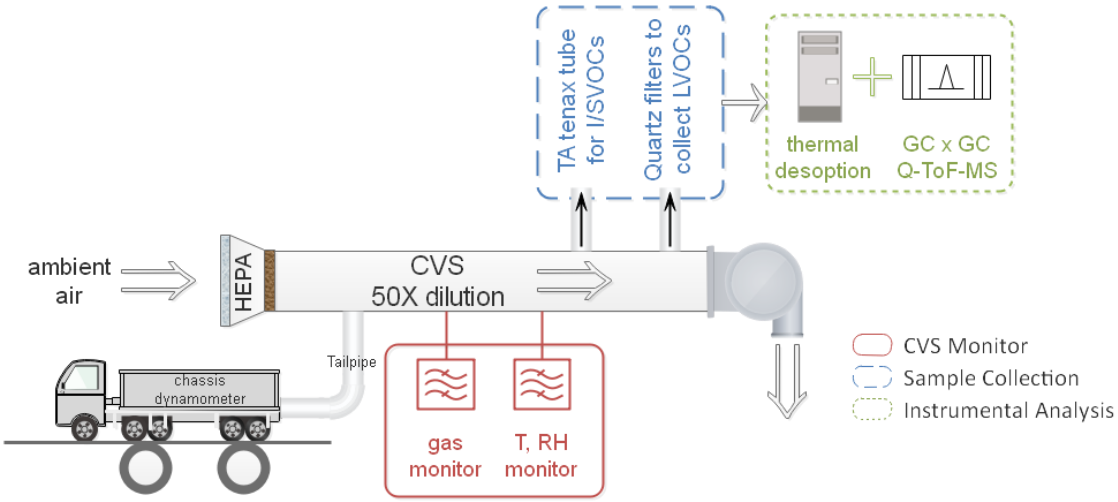

Figure S1. Experiment diagram to collect and characterize vehicle emissions. The constant volume sampler (CVS) system, sample collection, and instrumental analysis are highlighted by different colours. The exhaust is drawn into the CVS system, from which multiple sampling trains are assembled for different analysis purposes.

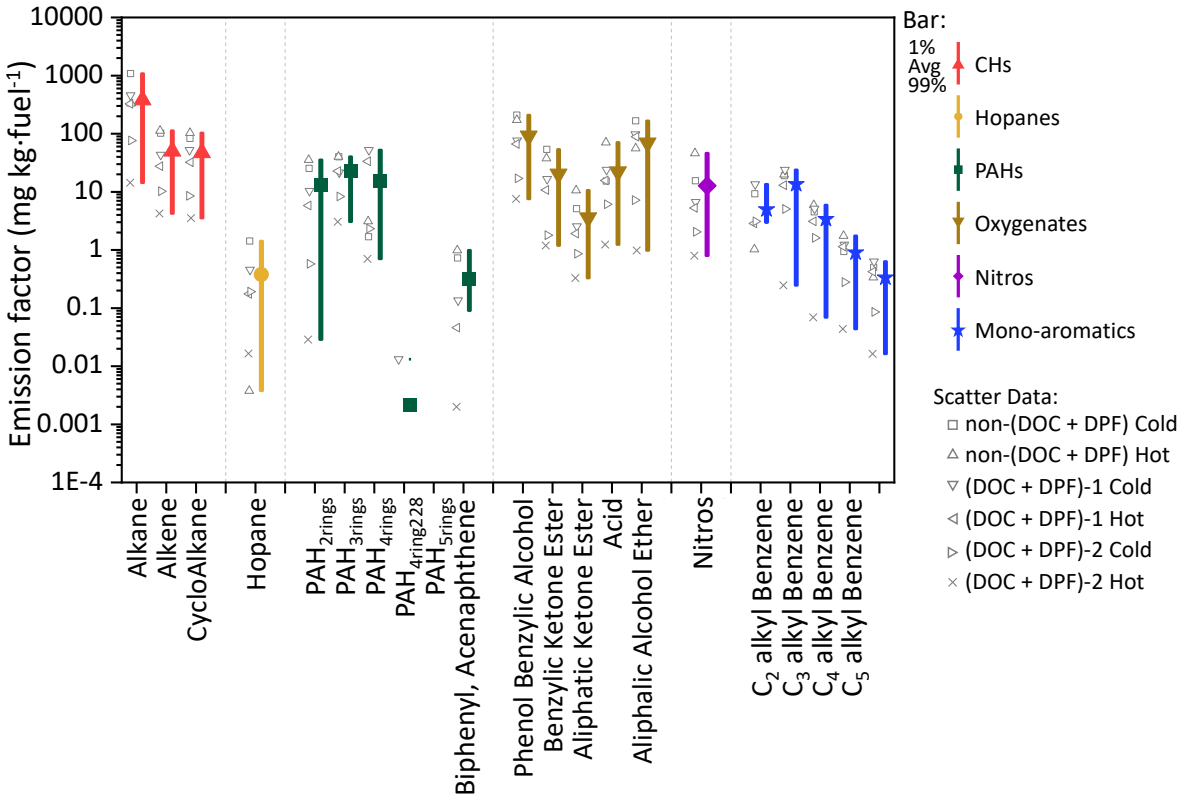

Figure S2. The measured emission factor (mg kg·fuel^{-1}) of the twenty-one categories of the HDDV-emitted I/SVOCs in the gas phase. Coloured-bars and coloured-scatters/shaped-scatters represent different organic species and driving cycles. The square dots in the middle of each bar denote the average value and the lower and upper boundaries of the bar denote the 1% and 99% percentile of the values.

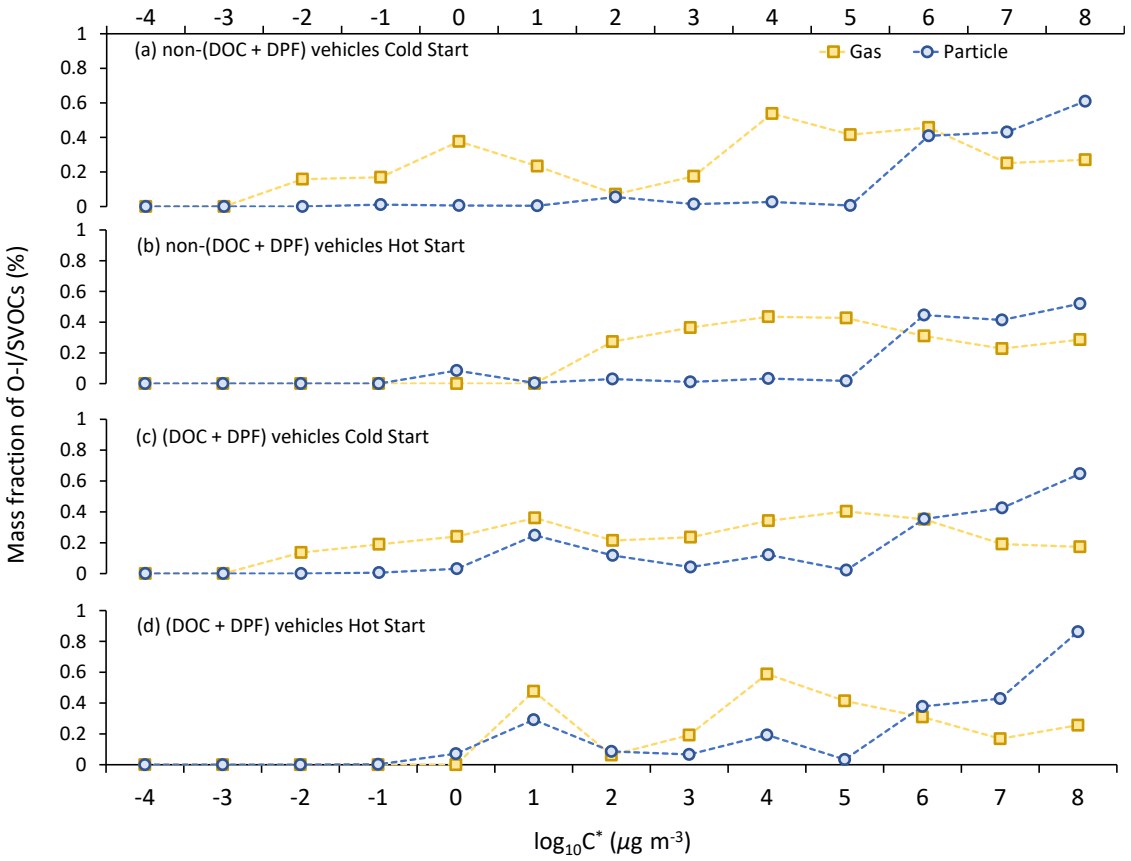

Figure S3. Mass fraction of O-I/SVOCs in the gas and particle phases in each volatility bins.

77 **Table S1. List of the authentic standards, corresponding internal standards, and the method detection limit (MDL).**

Name	Formula	Internal Standard	1st RT (s)	2nd RT (s)	MDL (μg)
		n-Alkane			
Tridecane	$C_{13}H_{28}$	*n*-Dodecane-d_{26}	1208	0.93	0.0005
Tetradecane	$C_{14}H_{30}$	*n*-Hexadecane-d_{34}	1368	0.94	0.0005
Pentadecane	$C_{15}H_{32}$	*n*-Hexadecane-d_{34}	1520	0.96	0.0005
Hexadecane	$C_{16}H_{34}$	*n*-Hexadecane-d_{34}	1660	0.97	0.0005
Heptadecane	$C_{17}H_{36}$	*n*-Hexadecane-d_{34}	1796	0.99	0.0005
Octadecane	$C_{18}H_{38}$	*n*-Eicosane-d_{42}	1924	1	0.0005
Nonadecane	$C_{19}H_{40}$	*n*-Eicosane-d_{42}	2044	1.02	0.0005
Eicosane	$C_{20}H_{42}$	*n*-Eicosane-d_{42}	2160	1.03	0.0005
Heneicosane	$C_{21}H_{44}$	*n*-Eicosane-d_{42}	2272	1.05	0.0005
Docosane	$C_{22}H_{46}$	*n*-Tetracosane-d_{50}	2376	1.06	0.0005
n-Tricosane	$C_{23}H_{48}$	*n*-Tetracosane-d_{50}	2480	1.08	0.0005
Tetracosane	$C_{24}H_{50}$	*n*-Tetracosane-d_{50}	2576	1.09	0.0005
Pentacosane	$C_{25}H_{52}$	*n*-Tetracosane-d_{50}	2672	1.11	0.0005
Hexacosane	$C_{26}H_{54}$	*n*-Octacosane-d_{58}	2760	1.13	0.0005
Heptacosane	$C_{27}H_{56}$	*n*-Octacosane-d_{58}	2848	1.15	0.0005
Octacosane	$C_{28}H_{58}$	*n*-Octacosane-d_{58}	2932	1.17	0.0005
n-Nonacosane	$C_{29}H_{60}$	*n*-Octacosane-d_{58}	3016	1.19	0.0005
n-Triacontane	$C_{30}H_{62}$	*n*-Octacosane-d_{58}	3092	1.23	0.0005
n-Hentriacontane	$C_{31}H_{64}$	*n*-Octacosane-d_{58}	3168	1.26	0.0005
n-Dotriacontane	$C_{32}H_{66}$	*n*-Octacosane-d_{58}	3244	1.3	0.0005
n-Tritriacontane	$C_{33}H_{68}$	*n*-Octacosane-d_{58}	3316	1.41	0.0005
n-Tetratriacontane	$C_{34}H_{70}$	*n*-Octacosane-d_{58}	3456	1.9	0.0005
n-Pentatriacontane	$C_{35}H_{72}$	*n*-Octacosane-d_{58}	3556	2.2	0.0005
n-Hexatriacontane	$C_{36}H_{74}$	*n*-Octacosane-d_{58}	3676	2.58	0.0005
n-Heptatriacontane	$C_{37}H_{76}$	*n*-Octacosane-d_{58}	3820	3.02	0.0005
		n-Alkene			
1-Tetradecene	$C_{14}H_{28}$	*n*-Dodecane-d_{26}	1356	0.99	0.00019
1-Cetene	$C_{16}H_{32}$	*n*-Hexadecane-d_{34}	1652	1.01	0.00019
1-Octadecene	$C_{18}H_{36}$	*n*-Hexadecane-d_{34}	1916	1.04	0.00018
1-Eicosene	$C_{20}H_{40}$	*n*-Eicosane-d_{42}	2152	1.07	0.00019
1-Docosene	$C_{22}H_{44}$	*n*-Eicosane-d_{42}	2420	1.22	0.00019
		Benzylic Ketone Ester			
Dimethyl phthalate	$C_{10}H_{10}O$	Phenanthrene-d_{10}	1512	2.58	0.0005
Diethyl Phthalate	$C_{12}H_{14}O$	Phenanthrene-d_{10}	1712	2.38	0.0005
		Cycloalkane			
Cyclohexane, octyl-	$C_{14}H_{28}$	*n*-Dodecane-d_{26}	1440	1.08	0.00018
Cyclohexane, decyl-	$C_{16}H_{32}$	*n*-Hexadecane-d_{34}	1736	1.12	0.00018
		PAH_{2rings}			
Naphthalene, 1-methyl-	$C_{11}H_{10}$	Naphthalene-d_8	1200	1.97	0.0005
Naphthalene, 2-methyl-	$C_{11}H_{10}$	Naphthalene-d_8	1228	2.04	0.0005
Naphthalene, 2-ethyl-	$C_{12}H_{12}$	Naphthalene-d_8	1368	1.99	0.0001
		PAH_{3rings}			
Acenaphthene	$C_{12}H_{10}$	Acenaphthene-d_{10}	1444	2.37	0.0005
Acenaphthylene	$C_{12}H_8$	Acenaphthene-d_{10}	1500	2.27	0.0005
Fluorene	$C_{13}H_{10}$	Acenaphthene-d_{10}	1640	2.32	0.0005
Phenanthrene	$C_{14}H_{10}$	Phenanthrene-d_{10}	1904	2.66	0.0005
Anthracene	$C_{14}H_{10}$	Phenanthrene-d_{10}	1916	2.65	0.0005
		PAH_{4rings}			
Fluoranthene	$C_{16}H_{10}$	Chrysene-d_{12}	2236	2.93	0.0005
Pyrene	$C_{16}H_{10}$	Chrysene-d_{12}	2292	3.14	0.0005
Benz[a]anthracene	$C_{18}H_{12}$	Chrysene-d_{12}	2640	3.31	0.0005
Chrysene	$C_{18}H_{12}$	Chrysene-d_{12}	2648	3.42	0.0005
		PAH_{5rings}			
Benzo[a]pyrene	$C_{20}H_{12}$	Chrysene-d_{12}	3012	0	0.0005
		Phenol Benzylic Alcohol			
Phenol	C_6H_6O	Phenanthrene-d_{10}	680	1.89	0.0005
Phenol, 2-methyl-	C_7H_8O	Phenanthrene-d_{10}	824	1.92	0.0005
p-Cresol	C_7H_8O	Phenanthrene-d_{10}	864	1.92	0.0005
Phenol, 2,4-dimethyl-	$C8H_{10}O$	Phenanthrene-d_{10}	1004	1.91	0.0005
		Nitros			
1-Propanamine, N-nitroso-N-propyl-	$C_6H_{14}N_2O$	Phenanthrene-d_{10}	860	1.91	0.0005
Benzene, nitro-	$C_6H_5NO_2$	Phenanthrene-d_{10}	888	2.36	0.0005

o-Nitroaniline	$C_6H_6N_2O_2$	Phenanthrene-d_{10}	1444	2.96	0.0005
Benzene, 2-methyl-1,3-dinitro-	$C_7H_6N_2O_4$	Phenanthrene-d_{10}	1524	2.88	0.0005
Benzene, 1-methyl-2,4-dinitro-	$C_7H_6N_2O_4$	Phenanthrene-d_{10}	1632	2.81	0.0005
Azobenzene	$C_{12}H_{10}N_2$	Phenanthrene-d_{10}	1756	2.4	0.0005

78

Table S2. A category-by-category EFs of I/SVOCs in the gas and particle phases for the non-(DOC + DPF) vehicles (Avg_{woAT}) and (DOC + DPF) vehicles (Avg_{wiAT}) and the removal efficiency.

	Particle				Gas			
	Avg_{all}	Avg_{wiAT}	Avg_{woAT}	Removal Efficiency	Avg_{all}	Avg_{wiAT}	Avg_{woAT}	Removal Efficiency
Alkane	15.70	0.25	46.60	0.99	381.68	218.64	707.75	0.69
Alkene	0.44	0.05	1.22	0.96	50.02	21.37	107.33	0.80
CycloAlkane	0.32	0.00	0.94	1.00	47.02	24.12	92.82	0.74
Hopane	0.21	0.00	0.62	1.00				
PAH_{2rings}	5.78	0.13	17.06	0.99	12.91	4.19	30.35	0.86
PAH_{3rings}	0.66	0.07	1.85	0.96	22.62	13.89	40.07	0.65
PAH_{4rings}	0.22	0.00	0.65	1.00	15.60	2.40	22.20	0.89
PAH_{5rings}	0.13	0.00	0.40	1.00				
Biphenyl, Acenaphthene	0.01	0.00	0.02	1.00	0.32	0.05	0.86	0.95
Phenol Benzylic Alcohol	1.05	0.15	2.83	0.95	91.42	41.79	190.70	0.78
Benzylic Ketone Ester	0.14	0.02	0.37	0.95	20.30	7.59	45.72	0.83
Acid	0.07	0.01	0.17	0.93	3.57	1.41	7.89	0.82
Aliphatic Ketone Ester	0.30	0.04	0.81	0.95	22.14	11.71	43.01	0.73
Aliphatic Alcohol Ether					69.45	48.60	111.16	0.56
C_2 alkyl Benzene					4.96	4.87	5.14	0.05
C_3 alkyl Benzene					13.51	10.54	19.43	0.46
C_4 alkyl Benzene					3.39	2.47	5.22	0.53
C_5 alkyl Benzene					0.90	0.67	1.35	0.50
C_6 alkyl Benzene					0.33	0.29	0.42	0.31
Nitros	0.40	0.05	1.08	0.95				
Total	25.01	0.73	73.57	0.99	772.94	438.14	1442.54	0.70

Table S3. The distribution of particulate I/SVOCs (mg km^{-1}) at low-speed stage for non-(DPF + DOC) vehicles separated by volatility bins and the O:C ratio.

$\log_{10}C^*$ (μg m^{-3})	O:C ratio											
	0-0.1	0.1-0.2	0.2-0.3	0.3-0.4	0.4-0.5	0.5-0.6	0.6-0.7	0.7-0.8	0.8-0.9	0.9-1.0	1.0-1.1	1.1-1.2
-4	4340.8	2033.1	2210.9	775.5	343.8	251.6	131.3	62.0	5.4	0.0	115.0	11.0
-3	5817.2	3185.1	2259.7	1283.1	467.0	320.5	240.2	77.9	41.3	0.0	35.4	21.9
-2	664.1	321.4	268.0	129.8	54.9	41.8	26.1	9.6	9.4	0.0	7.4	0.0
-1	226.1	38.3	46.6	16.3	13.4	11.0	1.2	2.9	0.0	0.0	0.0	1.1
0	66.2	17.1	0.7	0.6	0.0	0.4	0.9	0.0	0.0	0.0	25.8	0.0
1	398.1	19.6	5.2	1.8	0.3	0.2	0.0	1.4	0.0	0.0	23.1	0.1
2	173.0	29.0	94.9	0.2	0.0	0.0	1.1	2.5	0.0	0.0	0.0	0.0
3	296.4	107.6	3.7	4.2	0.8	3.5	0.0	0.0	0.0	0.0	0.0	0.0
4	108.6	12.7	43.6	26.7	2.1	0.0	0.0	0.0	0.0	0.0	0.0	0.0
5	47.3	22.8	83.5	87.2	28.3	201.4	14.6	3.0	0.0	0.0	0.0	0.0
6	460.3	197.1	116.3	30.9	29.0	15.2	0.0	0.0	0.0	0.0	0.0	0.0
7	887.8	715.4	215.8	200.8	39.0	163.4	0.0	0.0	0.0	0.0	0.0	0.0
8	89.4	158.2	11.3	7.7	32.3	44.7	36.0	12.6	0.0	0.0	6.9	0.0
9	806.7	49.7	4.2	103.4	13.7	259.4	45.1	0.0	0.0	0.0	17.3	0.0

Table S4. The distribution of particulate I/SVOCs (mg km^{-1}) at middle-speed stage for non-(DPF + DOC) vehicles separated by volatility bins and the O:C ratio.

$\log_{10}C^*$ ($\mu g\ m^{-3}$)	O:C ratio											
	0-0.1	0.1-0.2	0.2-0.3	0.3-0.4	0.4-0.5	0.5-0.6	0.6-0.7	0.7-0.8	0.8-0.9	0.9-1.0	1.0-1.1	1.1-1.2
-4	0.1	0.0	0.0	0.0	0.0	0.0	0.0	0.0	0.0	0.0	0.0	0.0
-3	0.0	0.1	0.0	0.0	0.0	0.1	0.1	0.0	0.0	0.0	0.0	0.0
-2	0.1	0.0	0.1	0.0	0.0	0.0	0.0	0.0	0.0	0.0	0.0	0.0
-1	0.3	0.6	0.0	0.0	0.0	0.0	0.0	0.0	0.0	0.0	0.0	0.0
0	4.6	0.6	0.4	0.0	0.0	0.0	0.0	0.0	0.0	0.0	0.0	0.0
1	9.2	0.3	1.5	0.2	0.0	0.0	0.0	0.0	0.0	0.0	0.0	0.0
2	23.8	3.9	4.7	0.4	0.0	0.0	0.0	0.0	0.0	0.0	0.0	0.0
3	109.8	11.0	1.6	0.7	0.1	0.0	0.0	0.0	0.0	0.0	0.0	0.0
4	172.4	5.0	4.2	3.3	0.1	0.0	0.5	0.0	0.0	0.0	0.0	0.0
5	66.9	3.9	8.6	19.0	2.1	18.0	1.7	0.0	0.0	0.0	0.3	0.0
6	81.0	17.4	11.9	2.8	1.1	1.6	0.5	0.0	0.0	0.0	0.0	0.0
7	42.6	20.3	17.6	5.7	0.4	10.0	0.0	0.0	0.0	0.0	0.3	0.0
8	2.8	9.6	1.9	1.4	0.5	4.4	0.8	0.0	0.0	0.0	0.5	0.0
9	3.1	1.0	1.5	3.8	1.1	12.5	0.2	3.1	0.0	0.0	1.9	0.0

Table S5. The distribution of particulate I/SVOCs (mg km^{-1}) at high-speed stage for non-(DPF + DOC) vehicles separated by volatility bins and the O:C ratio.

$\log_{10}C^*$ ($\mu g\ m^{-3}$)	O:C ratio											
	0-0.1	0.1-0.2	0.2-0.3	0.3-0.4	0.4-0.5	0.5-0.6	0.6-0.7	0.7-0.8	0.8-0.9	0.9-1.0	1.0-1.1	1.1-1.2
-4	0.0	0.0	0.0	0.0	0.0	0.0	0.0	0.0	0.0	0.0	0.0	0.0
-3	0.3	0.1	0.1	0.0	0.0	0.0	0.0	0.0	0.0	0.0	0.0	0.0
-2	0.3	0.1	0.0	0.0	0.0	0.0	0.0	0.0	0.0	0.0	2.4	0.0
-1	0.6	0.0	0.1	0.0	0.0	0.0	0.0	0.0	0.0	0.0	0.0	0.0
0	3.1	0.3	0.0	0.0	0.0	0.0	0.0	0.0	0.0	0.0	3.7	0.0
1	2.6	2.1	0.4	0.0	0.0	0.0	0.0	0.0	0.0	0.0	0.0	0.0
2	10.1	1.4	4.4	0.1	0.0	0.0	0.0	0.0	0.0	0.0	0.0	0.0
3	45.5	3.7	1.1	0.2	0.0	0.1	0.0	0.0	0.0	0.0	0.0	0.0
4	37.4	2.0	2.3	1.4	0.2	0.1	0.0	0.0	0.0	0.0	0.0	0.0
5	8.3	1.5	4.1	5.3	0.9	17.0	0.7	0.0	0.0	0.0	0.0	0.0
6	17.7	8.4	6.2	1.9	0.3	0.0	0.0	0.0	0.0	0.0	0.0	0.0
7	21.1	11.7	5.1	4.0	0.0	11.3	0.1	0.0	0.0	0.0	0.0	0.0
8	2.0	5.7	0.2	0.2	0.3	1.2	0.7	0.0	0.0	0.0	0.4	0.0
9	7.1	0.8	0.5	4.0	0.6	8.5	0.2	7.5	0.0	0.0	0.4	0.0

Table S6. The distribution of particulate I/SVOCs (mg km^{-1}) at whole driving cycle (W_cold) for non-(DPF + DOC) vehicles separated by volatility bins and the O:C ratio.

$\log_{10}C^*$ ($\mu g\ m^{-3}$)	O:C ratio											
	0-0.1	0.1-0.2	0.2-0.3	0.3-0.4	0.4-0.5	0.5-0.6	0.6-0.7	0.7-0.8	0.8-0.9	0.9-1.0	1.0-1.1	1.1-1.2
-4	121.0	56.7	61.6	21.6	9.6	7.0	3.7	1.7	0.1	0.0	3.2	0.3
-3	162.3	88.8	63.1	35.8	13.0	9.0	6.7	2.2	1.2	0.0	1.0	0.6
-2	18.7	9.0	7.5	3.6	1.5	1.2	0.7	0.3	0.3	0.0	1.3	0.0
-1	6.7	1.4	1.4	0.5	0.4	0.3	0.0	0.1	0.0	0.0	0.0	0.0
0	5.6	0.9	0.2	0.0	0.0	0.0	0.0	0.0	0.0	0.0	2.5	0.0
1	16.9	1.7	1.0	0.2	0.0	0.0	0.0	0.0	0.0	0.0	0.6	0.0
2	21.4	3.4	7.1	0.2	0.0	0.0	0.0	0.1	0.0	0.0	0.0	0.0
3	84.2	10.2	1.4	0.5	0.1	0.2	0.0	0.0	0.0	0.0	0.0	0.0
4	106.0	3.8	4.4	3.0	0.2	0.1	0.3	0.0	0.0	0.0	0.0	0.0
5	38.3	3.3	8.5	14.3	2.2	22.6	1.6	0.1	0.0	0.0	0.1	0.0
6	61.3	18.1	12.1	3.1	1.5	1.2	0.2	0.0	0.0	0.0	0.0	0.0
7	55.8	35.5	17.2	10.3	1.3	14.9	0.0	0.0	0.0	0.0	0.1	0.0
8	4.8	11.9	1.3	1.0	1.3	4.0	1.7	0.4	0.0	0.0	0.7	0.0
9	27.4	2.3	1.1	6.7	1.2	17.5	1.4	5.1	0.0	0.0	1.6	0.0

Table S7. The distribution of particulate I/SVOCs (mg km^{-1}) at whole driving cycle (W_hot) for non-(DPF + DOC) vehicles separated by volatility bins and the O:C ratio.

$\log_{10}C^*$ ($\mu g\ m^{-3}$)	O:C ratio											
	0-0.1	0.1-0.2	0.2-0.3	0.3-0.4	0.4-0.5	0.5-0.6	0.6-0.7	0.7-0.8	0.8-0.9	0.9-1.0	1.0-1.1	1.1-1.2
-4	12.04	0.00	0.42	0.00	0.00	0.00	0.00	0.00	0.00	0.00	0.00	0.00
-3	25.58	1.02	0.00	0.00	0.15	0.26	0.00	0.00	0.00	0.00	0.00	0.00
-2	11.38	0.00	0.00	0.00	0.00	0.00	0.19	0.00	0.00	0.00	0.00	0.00
-1	3.84	0.12	0.06	0.00	0.00	0.00	0.00	0.00	0.00	0.00	0.00	0.00
0	2.91	0.73	0.02	0.00	0.00	0.07	0.02	0.00	0.00	0.00	0.00	0.00
1	2.15	0.78	0.13	0.02	0.00	0.05	0.00	0.00	0.00	0.00	0.00	0.00
2	8.52	2.37	4.35	0.33	0.00	0.00	0.11	0.00	0.00	0.00	0.00	0.00
3	17.01	3.75	0.30	0.43	0.08	0.05	0.00	0.00	0.00	0.00	0.00	0.00
4	6.99	1.66	1.78	1.10	0.09	0.01	0.00	0.00	0.00	0.00	0.00	0.00
5	4.09	6.93	8.11	1.24	1.49	5.54	0.86	0.00	0.00	0.00	0.02	0.00
6	12.13	5.50	8.94	1.02	1.26	0.49	0.00	0.00	0.00	0.00	0.00	0.00
7	8.92	4.75	1.17	2.45	0.21	1.60	0.19	0.00	0.00	0.00	0.00	0.00
8	0.30	3.21	0.09	0.00	0.31	0.00	0.82	0.00	0.00	0.00	0.00	0.00
9	0.81	1.44	0.17	1.41	1.27	2.23	0.54	0.00	0.00	0.00	0.29	0.00

Table S8. The distribution of particulate I/SVOCs (mg km^{-1}) at low-speed stage for (DPF + DOC) vehicles separated by volatility bins and the O:C ratio.

$\log_{10}C^*$ ($\mu g\ m^{-3}$)	O:C ratio											
	0-0.1	0.1-0.2	0.2-0.3	0.3-0.4	0.4-0.5	0.5-0.6	0.6-0.7	0.7-0.8	0.8-0.9	0.9-1.0	1.0-1.1	1.1-1.2
-4	3.0	0.0	1.5	0.9	0.0	11.1	0.0	0.7	0.0	0.0	0.0	0.0
-3	9.2	2.5	2.8	2.2	0.5	0.0	0.3	0.0	0.0	0.0	0.0	0.0
-2	25.7	0.7	0.3	0.3	0.3	0.0	0.0	1.2	0.0	0.0	0.2	0.0
-1	27.8	4.8	0.7	1.0	0.3	0.0	0.0	0.0	0.1	0.0	0.0	0.0
0	83.8	6.9	3.0	0.4	0.1	2.1	1.0	0.2	0.0	0.0	0.5	0.0
1	46.9	29.1	9.5	7.6	3.0	1.3	1.2	0.2	0.2	0.0	0.2	0.0
2	99.2	35.2	115.4	3.5	1.3	0.2	2.7	0.7	0.1	0.0	8.4	0.0
3	328.0	48.3	10.0	5.3	0.7	7.8	0.3	0.3	0.0	0.0	0.2	0.0
4	132.2	10.8	41.6	49.6	2.0	0.3	0.4	0.0	0.0	0.0	0.2	0.0
5	87.7	12.2	49.9	108.9	17.2	115.5	4.1	0.3	0.0	0.0	0.4	0.0
6	408.6	237.5	74.7	32.8	17.8	5.2	2.2	0.0	0.0	0.0	0.0	0.0
7	1365.3	662.0	222.4	57.6	6.3	132.4	4.4	1.5	0.0	0.0	1.8	0.0
8	77.8	302.8	3.4	1.2	9.7	52.1	4.9	0.8	0.0	0.0	1.8	0.0
9	294.2	26.2	33.5	91.2	18.9	216.5	29.2	0.0	0.0	0.0	34.8	0.0

Table S9. The distribution of particulate I/SVOCs (mg km^{-1}) at middle-speed stage for (DPF + DOC) vehicles separated by volatility bins and the O:C ratio.

$\log_{10}C^*$ ($\mu g\ m^{-3}$)	O:C ratio											
	0-0.1	0.1-0.2	0.2-0.3	0.3-0.4	0.4-0.5	0.5-0.6	0.6-0.7	0.7-0.8	0.8-0.9	0.9-1.0	1.0-1.1	1.1-1.2
-4	1.2	0.9	0.6	0.6	0.0	2.4	0.0	0.0	0.0	0.0	0.0	0.0
-3	1.4	0.4	0.2	0.2	0.1	3.6	0.0	0.0	0.0	0.0	0.0	0.0
-2	1.2	0.1	0.0	0.0	0.0	4.1	0.0	0.0	0.0	0.0	0.0	0.0
-1	1.3	0.1	0.0	0.1	0.0	0.1	0.0	0.0	0.0	0.0	1.7	0.0
0	13.4	0.4	0.4	0.1	0.2	0.0	0.3	0.0	0.0	0.0	0.3	0.0
1	3.5	4.8	1.0	0.2	0.0	0.1	0.0	0.0	0.0	0.0	1.0	0.0
2	10.7	3.2	5.6	0.3	0.0	0.0	0.0	0.0	0.0	0.0	0.0	0.0
3	12.4	5.6	0.7	0.6	0.0	0.4	0.0	0.0	0.0	0.0	0.0	0.0
4	6.0	0.8	2.9	8.5	0.1	0.0	0.0	0.0	0.0	0.0	0.0	0.0
5	5.1	2.2	7.9	9.9	2.2	15.6	1.8	0.0	0.1	0.0	0.0	0.0
6	21.4	18.6	11.5	3.5	2.8	1.3	0.8	0.1	0.0	0.0	0.1	0.0
7	39.3	28.2	24.9	6.2	0.7	7.5	0.4	0.0	0.0	0.0	0.0	0.0
8	8.7	14.5	3.5	1.0	1.9	3.7	1.3	0.0	0.0	0.0	0.1	0.0
9	11.7	3.4	2.2	3.8	0.7	14.1	1.5	0.5	0.0	0.0	1.7	0.0

Table S10. The distribution of particulate I/SVOCs (mg km^{-1}) at high-speed stage for (DPF + DOC) vehicles separated by volatility bins and the O:C ratio.

$\log_{10}C^*$ (μg m^{-3})	O:C ratio											
	0-0.1	0.1-0.2	0.2-0.3	0.3-0.4	0.4-0.5	0.5-0.6	0.6-0.7	0.7-0.8	0.8-0.9	0.9-1.0	1.0-1.1	1.1-1.2
-4	1.6	0.4	0.1	0.3	0.0	5.2	0.0	0.0	0.0	0.0	0.0	0.0
-3	1.0	0.3	0.3	0.2	0.0	3.9	0.0	0.0	0.0	0.0	0.0	0.0
-2	1.0	0.0	0.1	0.0	0.0	0.5	0.0	0.0	0.0	0.0	0.0	0.0
-1	1.1	0.0	0.0	0.1	0.0	0.1	0.0	0.0	0.0	0.0	0.0	0.0
0	3.7	0.3	0.1	0.1	0.0	0.1	0.1	0.0	0.0	0.0	4.0	0.0
1	1.6	2.4	0.4	0.2	0.0	0.1	0.0	0.0	0.0	0.0	0.5	0.0
2	7.5	3.3	11.8	0.5	0.0	0.0	0.1	0.0	0.0	0.0	1.4	0.0
3	17.2	3.6	0.7	0.4	0.1	0.1	0.0	0.0	0.0	0.0	0.0	0.0
4	6.0	0.7	2.3	8.3	0.0	0.1	0.0	0.0	0.0	0.0	0.0	0.0
5	5.9	1.1	5.0	16.0	1.5	20.9	2.2	0.0	0.0	0.0	0.1	0.0
6	19.5	18.0	11.2	3.3	3.8	1.4	0.8	0.0	0.0	0.0	0.1	0.0
7	56.9	45.6	29.1	4.9	0.3	15.6	0.7	0.5	0.0	0.0	0.3	0.2
8	4.0	11.2	1.2	0.6	0.8	1.9	1.5	0.1	0.0	0.0	0.3	0.0
9	7.3	1.9	2.7	6.0	1.2	8.9	2.9	0.3	0.0	0.0	5.6	0.0

Table S11. The distribution of particulate I/SVOCs (mg km^{-1}) at whole driving cycle (W_cold) for (DPF + DOC) vehicles separated by volatility bins and the O:C ratio.

$\log_{10}C^*$ (μg m^{-3})	O:C ratio											
	0-0.1	0.1-0.2	0.2-0.3	0.3-0.4	0.4-0.5	0.5-0.6	0.6-0.7	0.7-0.8	0.8-0.9	0.9-1.0	1.0-1.1	1.1-1.2
-4	1.5	0.6	0.4	0.5	0.0	4.0	0.0	0.0	0.0	0.0	0.0	0.0
-3	1.4	0.4	0.3	0.2	0.0	3.6	0.0	0.0	0.0	0.0	0.0	0.0
-2	1.8	0.1	0.0	0.0	0.0	2.2	0.0	0.0	0.0	0.0	0.0	0.0
-1	1.9	0.2	0.0	0.2	0.0	0.1	0.0	0.0	0.0	0.0	0.8	0.0
0	10.7	0.6	0.3	0.1	0.1	0.1	0.2	0.0	0.0	0.0	2.1	0.0
1	3.8	4.3	0.9	0.4	0.1	0.1	0.1	0.0	0.0	0.0	0.8	0.0
2	11.7	4.2	11.6	0.5	0.1	0.0	0.1	0.0	0.0	0.0	0.9	0.0
3	23.5	5.8	1.0	0.6	0.1	0.5	0.0	0.0	0.0	0.0	0.0	0.0
4	9.5	1.0	3.7	9.5	0.1	0.0	0.0	0.0	0.0	0.0	0.0	0.0
5	7.8	1.9	7.7	15.6	2.3	20.9	2.0	0.0	0.0	0.0	0.1	0.0
6	31.3	24.4	13.1	4.2	3.7	1.5	0.8	0.1	0.0	0.0	0.1	0.0
7	84.7	54.2	32.4	7.0	0.6	14.9	0.6	0.3	0.0	0.0	0.2	0.1
8	8.4	20.9	2.4	0.8	1.6	4.2	1.5	0.1	0.0	0.0	0.2	0.0
9	17.5	3.3	3.3	7.3	1.5	17.3	3.0	0.4	0.0	0.0	4.5	0.0

Table S12. The distribution of particulate I/SVOCs (mg km^{-1}) at whole driving cycle (W_hot) for (DPF + DOC) vehicles separated by volatility bins and the O:C ratio.

$\log_{10}C^*$ (μg m^{-3})	O:C ratio											
	0-0.1	0.1-0.2	0.2-0.3	0.3-0.4	0.4-0.5	0.5-0.6	0.6-0.7	0.7-0.8	0.8-0.9	0.9-1.0	1.0-1.1	1.1-1.2
-4	0.21	0.26	0.10	0.05	0.00	5.27	0.00	0.00	0.00	0.00	0.00	0.00
-3	0.38	0.09	0.06	0.00	0.02	1.74	0.00	0.07	0.01	0.00	0.00	0.00
-2	0.38	0.03	0.02	0.00	0.00	0.29	0.00	0.00	0.00	0.00	0.00	0.00
-1	0.43	0.06	0.01	0.04	0.00	0.04	0.00	0.00	0.00	0.00	5.44	0.00
0	2.34	0.31	0.11	0.03	0.00	0.00	0.00	0.00	0.00	0.00	1.13	0.00
1	1.47	0.88	0.10	0.08	0.01	0.03	0.00	0.01	0.01	0.00	0.74	0.00
2	7.49	2.15	6.00	0.15	0.04	0.01	0.05	0.00	0.01	0.00	0.36	0.00
3	7.83	6.48	0.51	0.52	0.07	0.19	0.01	0.00	0.00	0.00	0.00	0.00
4	3.58	0.48	1.93	3.60	0.06	0.03	0.00	0.00	0.00	0.00	0.01	0.00
5	7.51	1.62	5.82	2.40	2.23	16.47	1.09	0.12	0.00	0.00	0.78	0.00
6	22.21	12.66	7.23	9.99	2.40	2.96	1.32	0.08	0.00	0.00	0.21	0.00
7	31.70	12.19	8.89	6.74	0.05	5.74	0.25	0.00	0.09	0.00	0.11	0.00
8	7.02	5.74	7.26	0.27	0.83	5.43	2.50	0.53	0.00	0.00	0.15	0.00
9	5.58	2.20	2.39	3.19	0.20	5.53	1.06	0.10	0.00	0.00	4.43	0.00

References:

Alam, M. S., Zeraati-Rezaei, S., Liang, Z., Stark, C., Xu, H., MacKenzie, A. R., & Harrison, R. M. (2018). Mapping and quantifying isomer sets of hydrocarbons (≥ C12) in diesel exhaust, lubricating oil and diesel fuel samples using GC × GC-ToF-MS. *Atmospheric Measurement Techniques, 11*(5), 3047-3058. doi:10.5194/amt-11-3047-2018

https://www.epa.gov/tsca-screening-tools/download-epi-suitetm-estimation-program-interface-v411. (2021, March 12, 2021). EPI Suite™ - Estimation Program Interface v4.11. Retrieved from https://www.epa.gov/tsca-screening-tools/download-epi-suitetm-estimation-program-interface-v411

Huo, Y., Guo, Z., Liu, Y., Wu, D., Ding, X., Zhao, Z., . . . Chen, J. (2021). Addressing Unresolved Complex Mixture of I/SVOCs Emitted From Incomplete Combustion of Solid Fuels by Nontarget Analysis. *Journal of Geophysical Research: Atmospheres, 126*(23). doi:10.1029/2021jd035835

May, A. A., Presto, A. A., Hennigan, C. J., Nguyen, N. T., Gordon, T. D., & Robinson, A. L. (2013a). Gas-particle partitioning of primary organic aerosol emissions: (1) Gasoline vehicle exhaust. *Atmospheric Environment, 77*, 128-139. doi:10.1016/j.atmosenv.2013.04.060

May, A. A., Presto, A. A., Hennigan, C. J., Nguyen, N. T., Gordon, T. D., & Robinson, A. L. (2013b). Gas-Particle Partitioning of Primary Organic Aerosol Emissions: (2) Diesel Vehicles. *Environmental Science & Technology, 47*(15), 8288-8296. doi:10.1021/es400782j

Zhao, Y., Nguyen, N. T., Presto, A. A., Hennigan, C. J., May, A. A., & Robinson, A. L. (2015). Intermediate Volatility Organic Compound Emissions from On-Road Diesel Vehicles: Chemical Composition, Emission Factors, and Estimated Secondary Organic Aerosol Production. *Environmental Science and Technology, 49*(19), 11516-11526. doi:10.1021/acs.est.5b02841